Pollution, 6(3): 581-595, Summer 2020
DOI: 10.22059/poll.2020.298554.755
Print ISSN: 2383-451X Online ISSN: 2383-4501
Web Page: https://jpoll.ut.ac.ir, Email: jpoll@ut.ac.ir

Response surface method Optimization of the Dyes Degradation using Zero-Valent Iron based Bimetallic Nanoparticle on the Bentonite Clay Surface

Sabouri, M. R.[1], Sohrabi, M. R.[1*] and Zeraatkar Moghaddam, A.[2]

1. Department of Chemistry, Islamic Azad University, North Tehran Branch, P.O. Box 1913674711, Tehran, Iran

2. Department of Chemistry College of Sciences, University of Birjand, P.O. Box 97175-615, Birjand, Iran

Received: 27.02.2020 Accepted: 27.05.2020

ABSTRACT: Immobilizing of zero-valent iron in mono- and bi-metallic systems on the bentonite clay surface as new nanocatalyst were synthesized and used to degrade model acidic dyes from aqueous media. The Fourier-transform infrared spectroscopy, scanning electron microscopy-energy dispersive X-ray spectroscopy, transmission electron microscopy, X-ray diffraction, and Brunauer-Emmett-Teller analysis were used to characterize the synthesized nanocomposites, which demonstrated successful loading of nanoscale Fe-Cu bi-metallic onto bentonite support. Different variables controlling the congo red, methyl orange and methyl red dyes degradation using zero-valent iron based bimetallic nanoparticle on the bentonite clay surface as new nanocatalyst were concurrently optimized through an experimental design. Basic evaluations proved the nanocatalyst quantity, medium pH, initial dye concentration, and contact time as the most important variables influencing the degradation phenomenon and hence a response surface methodology based on the central composite design was conducted to determine the relations between the variables and the degradation efficiencies. The statistical factors (e.g. R^2 and F-value) of the derived models were considered. Using response surface plots obtained through the models, the effects of the variables on the degradation efficiencies for each dye were assessed. Also, the Nelder-Mead non-linear optimizations were performed and the optimal degradation efficiencies at a 95% confidence level were determined which were found to comply with the respective experimental response values.

Keywords: Pollutant; Nanocatalyst; Characterization; Degradation; Modeling.

INTRODUCTION[*]

Being one of the chief consumers of different dyes, the textile industry is held responsible for a great deal of water contaminations. Almost none of the azo dyes are biodegradable which gives rise to long term environmental problems (Hao et al., 2000). As examples of these azo dyes, Congo red (CR), methyl orange (MO), and methyl red (MR) are known as potential sources of carcinogenic, mutagenic and teratogenic damages to humans (Moghaddam et al., 2020; Sabouri et al., 2020). On the other hand, dyes are not easily tough to degraded and their removal requires in nature and require more other advanced alternative techniques for their removal (Hajjaji et al., 2013). Thus various chemical, physical and biological treatment methods procedures

* Corresponding Author, Email: m.r.sohrabi2018@gmail.com

have been developed to this end for the removal of dyes from aqueous solutions. These methods include treatments include precipitation, coagulation-flocculation, reverse osmosis, oxidation with ozone, chlorine or hydrogen peroxide, use application of anion exchange membranes and bacterial cells (Belessi et al., 2009). Adsorption is one of another the most very promising and hence widely used scenario is adsorption of promising and widely used techniques for the removal synthetic dyes from wastewaters (Mittal and Ray, 2016; Zeraatkar Moghaddam et al., 2018, 2019), which has been found to be proven to be a promising and very cost-effective method. Therefore, the search for novel and efficient adsorbents with high adsorption capacities is still a competitive are of research (Behbahani et al., 2014, 2013; Bojdi et al., 2014; Kurniawan et al., 2012). However, in adsorption methods, the concentrated dye wastewater is also produced by regeneration of adsorbents and it needs further treatment and disposal which is the important drawbacks of these method.

Catalytic method for dyes degradation were recently considered (Bao et al., 2020; Chakraborty et al., 2019; Diao et al., 2016; Karthiga et al., 2015; Sahoo et al., 2015; Sahoo and Patra, 2018; Salama et al., 2018) which compared to other treatment technologies, the efficiency is higher, there is a selectivity toward nontoxic products, relatively mild conditions are required, and the operation is easier (Diao et al., 2016; Jouali et al., 2019; Marković et al., 2019; Vijai Anand et al., 2019). Different materials have been used for catalytic dyes degradation to develop effective and selective catalysts (Diao et al., 2016; O'Carroll et al., 2013; Salama et al., 2018; Shubair et al., 2018).

In the light of the various promises of the application of nano-scale particles, e.g. the application of nano-sized materials in the treatment of wastewater various nano-adsorbents and nanocatalysts have been evaluated for removing dyes from wastewaters. The improvements observed with nano-sized materials are associated with the enhancements in the surface area and number of active sites present on the surface of nano-materials leading to improved absorption and catalytic capacities of such nanomaterials.

It is also a fact that optimizing of the treatment process can lead to practical outcomes. Various statistical procedures have been applied to optimize such procedures. These include the Taguchi, genetic algorithm, neural network, iterative mathematical search, metaheuristic search, heuristic search, simulated annealing and response surface methodologies (RSM) (Asfaram et al., 2016; Derringer and Suich, 1980; Montgomery, 2012). The last method in the list, i.e. RSM, is a statistical approach based on using experimental quantitative data to solve multivariate equations and determine the optimal conditions required for the best response. The most common class of RSM is known as the central composite design (CCD). CCD is based on (i) design of the experiments, (ii) estimation of the coefficients in a mathematical model, and eventually (iii) predicting the response and validation of the model.

The current work involved preparing Fe-Cu and Ben@Fe-Cu as bimetallic nanocatalyst and evaluating them for catalytic removing of CR, MO, and MR in aqueous solutions. The composition and morphology of the synthesized nanomaterials were satisfactory. In a next step of this study, experimental design was used to optimize the treatment process. The interactions among the parameters and the optimal condition were estimated using a limited number of test runs and RSM was used to determine a reliable model under CCD.

MATERIAL AND METHODS

Adjusting and reading solution pH was carried out by a SCHOTT pH-meter equipped with a glass electrode. By an Analytikjena, Specord 210 UV/Vis, the

concentration of the each dyes in aqueous samples was determined at their appropriate λ_{max}. By a Philips CM-30 transmission electron microscope, a Perkin-Elmer Spectrum 65 Fourier transform infrared spectrometer, Bruker AXS-D8 powder X-ray diffractometer, TESCAN Vega3 scanning electron microscope, and Belsorp min BET, the characterizations of the synthesized nanocomposites were achieved. No further purification was carried out for purchased chemicals. The typical CR, MO and MR dyes were purchased from Sigma-Aldrich Co. An appropriate amount of each dyes was dissolved in doubly distilled water (DDW) to prepare the stock solution, and then it was diluted with DDW to reach the goal concentrations. By addition of appropriate amounts of either 0.1 M HCl or 0.1 M NaOH solutions, the pH of the solutions was adjusted to desired value.

In synthesis of nano-sized materials, the co-precipitation method was used to synthesize NZVI. Here, sodium borohydride ($NaBH_4$) was used to reduce iron chloride ($FeCl_3.6H_2O$) salt in a three-necked volumetric flask using a magnetic stirrer and flow of inert noble gas. In a 30 ml mixture of ethanol and water, 0.5406 g of $FeCl_3.6H_2O$ was dissolved, 4:1 (v/v). Then, 0.3783 g of $NaBH_4$ was dissolved in 100 mL of water in a separate beaker, and the latter solution was dropped to the first one till to complete precipitation, in the presence of the argon gas, which was bubbled through the setup. Nitrogen or argon flow is necessary due to the high tendency of formed nanoparticles to oxidation. According to the following reaction, solid black nanoparticles will appear after the addition of first drops of $NaBH_4$ to the solution. The formation of perfect NZVI is granted by the extra amount of $NaBH_4$.

$$2FeCl_3 + 6NaBH_4 + 18H_2O \rightarrow 2Fe^0 + 6NaCl + 6B(OH)_3 + 21H_2 \quad (1)$$

The obtained solution was stirred for 10 min after the addition of all $NaBH_4$. Then, the precipitate was separated from the solution using an external magnetic field, washed three times with ethanol, in a vacuum oven, the nanoparticles were dried at 80 °C, and finally, they were kept in a sealed glass vessel filled with argon for storage. The liquid-phase reduction method was applied to immobilize the NZVI on bentonite support (Be@Fe) adding 2.00 g bentonite to a 50 mL mixture solution of ethanol and water, 4:1(v/v), containing 9.66 g $FeCl_3.6H_2O$ which was stirred for 30 min. Then, a 100 mL solution having 3.54 g of $NaBH_4$ was dropped while the first solution was stirring under argon gas flow till a black precipitate appeared. At room temperature, stirring was continued for 20 more minutes. Then, a magnet was used to separate the black precipitate from the solution, washed three times with ethanol, and finally, in a vacuum oven, Be@Fe nanoparticles were dried at 80 °C. A similar procedure (section E) was applied to synthesize them. The except was that, before drying Be@Fe nanoparticles, a solution which was prepared from dissolving 0.786 g of $CuSO_4.5H_2O$ in 200 mL water was dropped to the washed Be@Fe nanoparticles, which were synthesized from the previous step. Then, keeping the temperature constant at 30 °C, argon gas was bubbled through the resulted mixture for 10 min, followed by using an external magnetic field to separate the solid phase and washing it three times with methanol. Finally, in the vacuum oven, bimetallic nanoparticles supported on bentonite (Be@Fe-Cu) were dried at 80 °C.

The dyes degradation experiments were performed in batch mode by adding desired amounts of the nanomaterials to 10 mL of CR, MO or MR solutions in 15 ml tubes lodged on a Lab Teatmet ST5 CAT shaker. After known periods of time, the resulting suspensions were passed through 0.45 μm syringe filters and the dye contents of the

liquid phases were determined using UV-Vis spectrophotometer. The dye degradation percentage (R%) and capacity (q, mg/g) of the tested nanomaterial in each experiment were calculated using the spectra data and the following equations:

$$R(\%) = \frac{C_0 - C_t}{C_0} \times 100 \quad (2)$$

$$q = \frac{C_0 - C_t}{m} V \quad (3)$$

C_o and C_t (mg/L) being the dye concentrations before the treatment and after time t. Also m (g) is the quantity Be@Fe-Cu amount and V (L) is the solution volume.

RESULTS AND DISCUSSION

The identification of synthesized Be@Fe-Cu nanocomposite was carried out using FT-IR, BET, XRD, TEM, SEM-EDX before the proposed nanocomposite could be used.

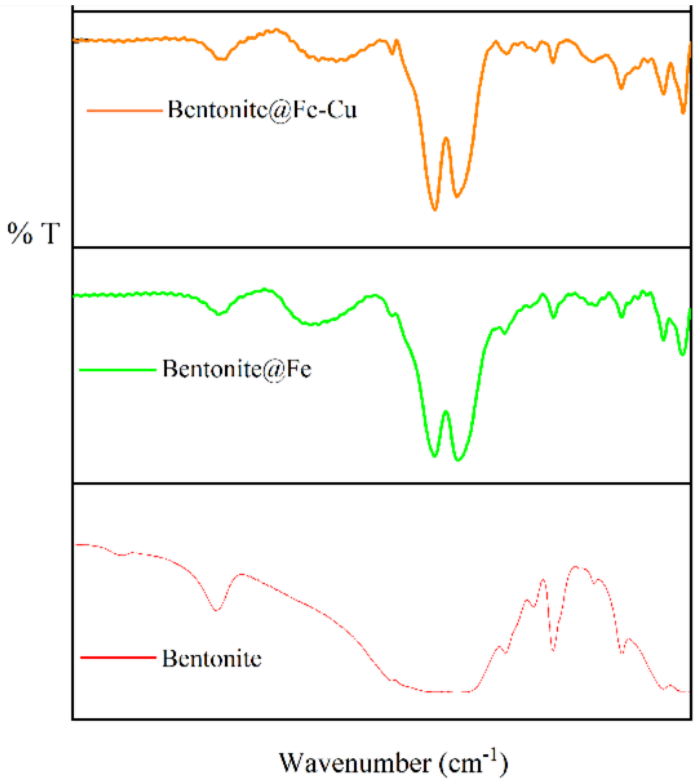

Fig. 1. FTIR spectra of bentonite, Be@Fe, and Be@Fe-Cu

Figure 1 presents the FT-IR spectra of bentonite, Be@Fe, and Be@Fe-Cu. Stretching and asymmetric bending vibration of O-H regarding absorbed water correspond to two absorption bands in 3439 and 1646 cm^{-1}, which are appearing in all spectra. Figure 1 also presents that in the bentonite FT-IR spectrum, stretching vibrations at 472 and 1074 cm^{-1} are related to the Si-O-Si band. At about 621 cm^{-1}, stretching vibrations of Al-O and Si-O could be observed. At 3630 cm^{-1}, stretching vibration of the O-H groups attached to metals (Al and Mg) exists. Band deformations are evident of at 523 and 795 cm^{-1} for Si-O-Al and Si-O, respectively, and at 1637 and 3428 cm^{-1} for O-H of water. Figure 1 presents that in the FT-IR spectra of Be@Fe, and Be@Fe-Cu, a new band has appeared in 1384 cm^{-1}, which attributes to surface adsorption of nZVI on bentonite. At 1230 and 1384 cm^{-1}, weak absorption bands are attributed to bending vibration of O-H in iron existing in bentonite surface.

In XRD, the pattern of scattered X-rays

is analyzed for a sample that is irradiated with an X-ray beam, which is a unique method to evaluate crystalline structure and phases, size, and shape of crystals, the distance between layers in the crystalline lattice, chemical composition and physical properties of materials. Determination of the approximate size of a crystal is possible with assigning the position and width of peaks in an XRD pattern according to the following Debye–Scherrer equation.

$$D = \frac{K\lambda}{\beta \cos\theta} \quad (4)$$

where D is crystal size, λ is x-ray wavelength, β is the full width at half-height of the peak in the rad, θ is diffraction angle, and K is a constant that its value varies between 0.89- 1.39 depending on the shape and crystalline structure which is 0.9 in the present study. Thus, the average crystallite size of synthesized products was calculated at about 29.4 nm. Here, investigation of the crystallinity and degree of the morphology of synthesized nanocomposites was carried out by implementing the XRD pattern. Figure 2 presents the XRD pattern of Be@Fe-Cu. NZVI formation was indicated by appeared peaks at 2θ of 45.8° and 64.1°. The existing peaks at 2θ of 35.7° and 56.6°-62.3° attribute to Fe_2O_3 and Fe_3O_4. These oxides are the result of an oxide layer formation onto the surface of nanoparticles exposed to the atmosphere. When the value of 2θ was 43.26° and 50.04°, CuO diffraction weak peaks appeared for Be@Fe-Cu illustrating CuO was coated on the Be@Fe-Cu. At 2θ=36.4°, the obvious Fe-O peak suggests that Fe_2O_3 could adhere to the Be@Fe-Cu surface similar to the XRD pattern of Ben@Fe-Cu. The diffraction peak at 2θ=61.1° is attributed to FeOOH, conveying that Ben@Fe-Cu could be oxidized to FeOOH. The immobilization of Fe-Cu nanoparticles in bentonite layers as indicated by the existence of Fe^0 main peak in the XRD pattern of all samples. The results of XRD analysis suggest that the desired substrates have been synthesized successfully.

Figure 3 presents TEM images for Ben@Fe-Cu. The average size of nanoparticles is less than 50 nm, and the resulted nanocomposite has been immobilized well on bentonite surface.

Figure 4 depicts layer by layer structure of bentonite where SEM image and EDX analysis of Ben@Fe-Cu nanocomposite have been presented. The nanoparticles are disaggregated. The presence of elements in Ben@Fe-Cu was also presented by the EDX analysis indicating successful synthesizing of the nanocomposites.

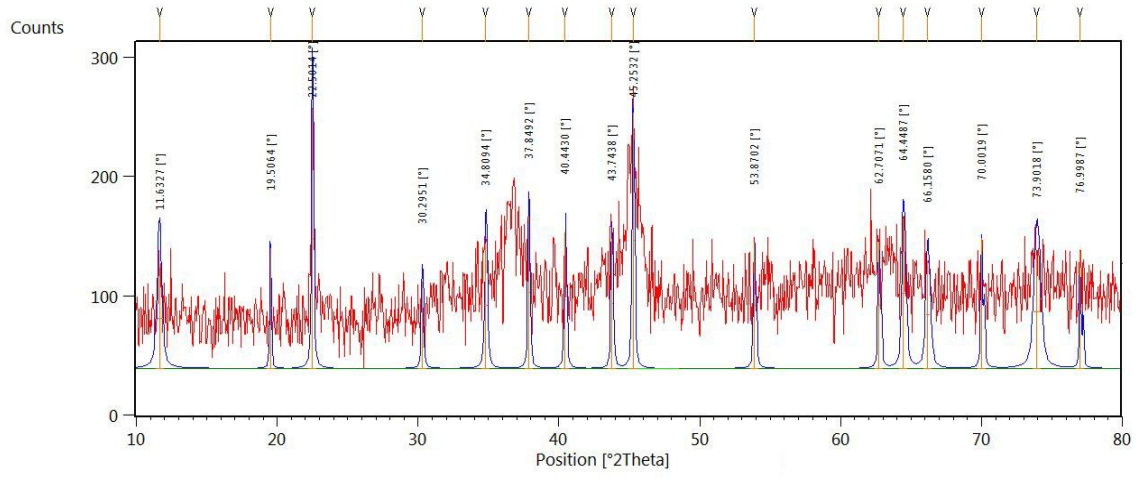

Fig. 2. XRD pattern of Ben@Fe-Cu

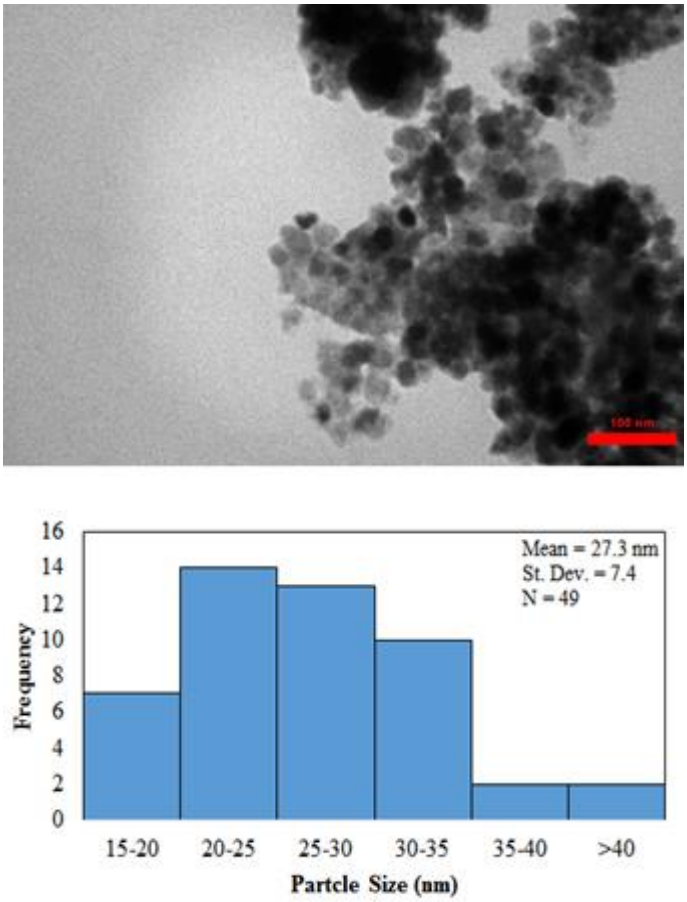

Fig. 3. TEM image and its particle size distribution for Be@Fe-Cu

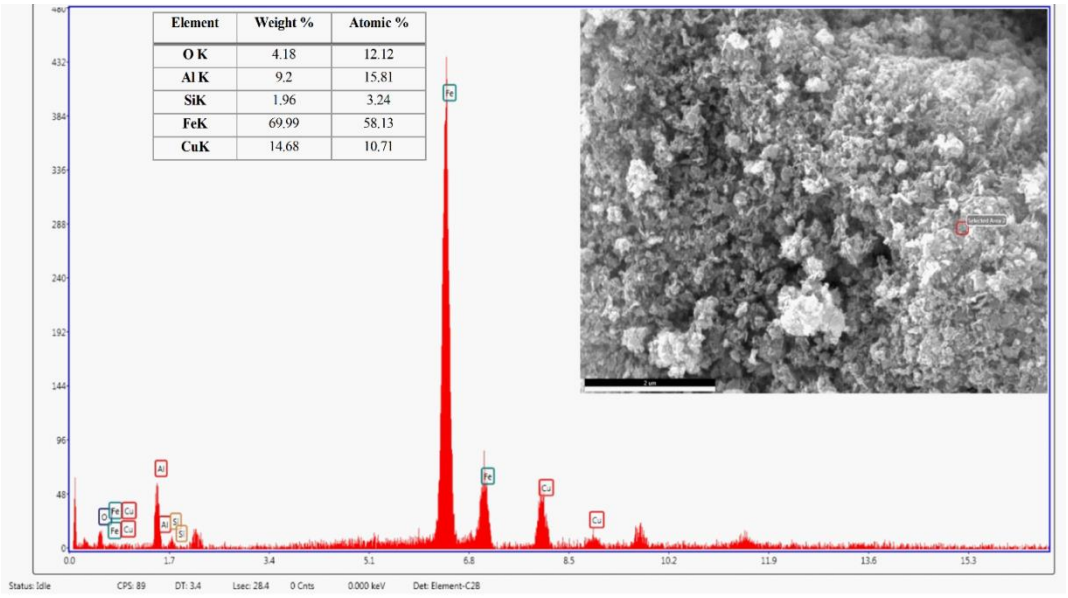

Fig. 4. SEM-EDX analysis for Be@Fe-Cu

Adsorption and desorption of N_2 were used to determine the specific surface area. For Ben@Fe-Cu, the BET surface areas were 45.6 m^2/g.

After successful characterization, the comparison between the synthesized nanocatalyst was done. First, by dissolving the appropriate amount of each dye in the water at pH =3, a 50 mL solution of 200 ppm CR or MO was prepared to evaluate the performance of these developed substrates. Then, it was dispensed of equally in five beakers, each containing 10 ml. Then, beakers were shaken at 210 rpm for 20 min when 50 mg from each substrate was poured into every beaker. As illustrated in Fig. 5, due to the presence of a negative charge on the surface of bentonite, which results in repulsion force between dyes and clay surface, the results showed that it had 0% degradation efficiency. NZVI possessed degradation efficiency for CR, MO and MR are reasonable values. Thus, the immobilization of these nanoparticles onto the bentonite surface as support increases the degradation efficiency of dyes. The nanoparticle aggregation is prevented by the presence of support, which leads to more particle dispersion in the system which in turn could improve degradation efficiency. Both oxidation and deactivation are impeded by the existence of the second metal into nanoparticles. The results suggest the better performance of Ben@Fe-Cu nano-catalysts in comparison to bentonite, nZVI, and Ben@Fe nanoparticles. Thus, Be@Fe-Cu was utilized in dye degradation and optimization step.

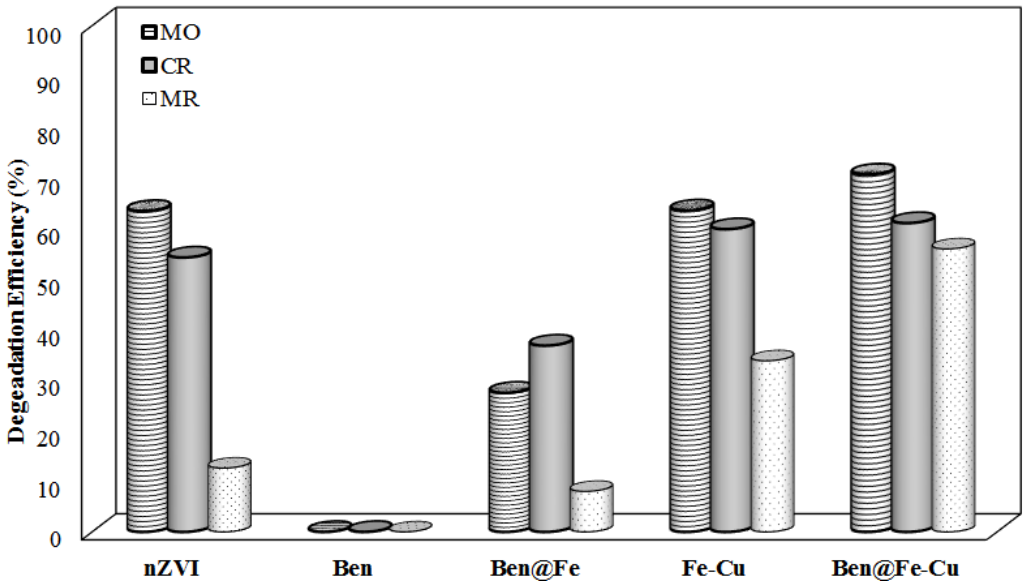

Fig. 5. Degradation efficiency of different synthesized nanomaterials

Univariate methodology is a common procedure, yet it suffers the disadvantages of being time and cost extensive and inability to consider the interactions of variables. On the other hand, multivariate techniques such as RSM are fast and efficient and can concurrently optimize more than one variable (Montgomery, 2012). As a class of RSMs, CCD provides an independent, rotatable technique for orthogonal and quadratic designs (Montgomery, 2012). In the case of dye degradation phenomena using Be@Fe-Cu, pH, nanocomposite quantity, initial dye concentration and time have been known as the most important variables (Zeraatkar Moghaddam et al., 2018), and hence this study was focused on optimizing these variables through CCD and next the effects of the variables on the response which contributed to building of a surface were studied through RSM. The relationships

between the response and these variables were graphically illustrated using a mathematical model. As a final point, the analysis of variance (ANOVA) was used to evaluate the model and the data.

Given the limited number of parameters they were not screened by factorial design, and hence CCD was directly used. A CCD approach for k factors, is commonly coded as (χ_1,..., χ_k), involving 3 parts, i.e. (i) a factorial design composed of a total of $n_f = 2^k$ points with $\chi_i = -1$or $\chi_i = +1$, for i =1,..., k coordinates; (ii) an axial part, involving $n_{ax} = 2k$ points with all coordinates being null except for the point with a certain value of α (or −α) ranging from 1 to √k; (iii) a total of n_c runs at the center of the experimental region to reach properties like orthogonality or rotatability to fit quadratic polynomials. To obtain a good estimate of the experimental error, the central points are generally repeated.

CCD can be made rotatable and orthogonal by choosing a suitable axial point α using the following expression:

$$\alpha = \sqrt[4]{N_f} \tag{5}$$

$$\alpha = \sqrt{\frac{\sqrt{(N_f + N_a + N_0)N_f} - N_f}{2}} \tag{6}$$

N_f, N_a and N_o being the numbers of factorial, axial and central points. Using Eq. (3), the axial spacing and N_o were determined to be ±2.0 and 6. For f variables, the number of design points required (N) can be determined using Eq. (7):

$$N = 2^f + 2f + N_0 \tag{7}$$

Consequently, 30 experiments were needed for the CCD design, and these were randomized into 3 blocks.

The results of ANOVA for the CCD design matrix are illustrated in Table 1. This table can be used to choose the suitable response surface models, their significances and terms. The table indicates the F-value to be 65.3 reflecting the significance of the model. Further the value of "p-values" less than 0.050 for a factor reflects the significance of its effect. A quadratic response surface model was chosen for fitting the experimental data. In the light of the higher F- and R-values as well as the lower lack of fit (LOF). The multiple linear regression (MLR) model was used in backward mode, to calculate the regression coefficients so as to eliminate the non-significant effects from the model. Based on what was said, the model for predicting the removal percentage of dyes using Be@Fe-Cu (in terms of the coded factors) was expressed using the expression below:

$$\begin{aligned}\text{MO degradation efficiency (\%)} &= 72.7 - 4.2A + 3.5B \\ &- 4.3C + 1.5D + 1.3AC \\ &- 2.3BC - 1.3A^2 - 1.8B^2 \\ &- 2.5D^2\end{aligned} \tag{8}$$

$$\begin{aligned}\text{CR degradation efficiency (\%)} &= 64.6 - 5.0A + 4.2B \\ &- 4.7C + 4.2D - 1.3A^2 \\ &- 3.1B^2 - 3.1D^2\end{aligned} \tag{9}$$

The F-values for LOF indicating it was not significant as opposed to the pure experimental error, and confirming the validity of the model. The calculations showed the respective values for R^2_{pred} and R^2_{adj} as being 0.90 for all investigated dyes.

The normal probability and studentized residual plots obtained for the catalytic removal process studied are presented in Fig. 6, where the straight line pattern indicates the normal distribution of the residuals. Also comparing the plots of externally studentized residuals against variables like the predicted values (not shown), run order (not shown), and factors (not shown), revealed an almost constant variance in the variable ranges for dyes removal.

Table 1. ANOVA Table

	Source	SS	df	MS	F Value	p-value
MO dye	Model	1619.56	14	115.68	17.62	< 0.0001
	A-Initial pH	423.36	1	423.36	64.49	< 0.0001
	B-Dose	302.46	1	302.46	46.07	< 0.0001
	C-Ci	436.91	1	436.91	66.55	< 0.0001
	D-Contact Time	54.60	1	54.60	8.32	0.0128
	AB	2.56	1	2.56	0.39	0.5431
	AC	27.56	1	27.56	4.20	0.0612
	AD	3.80	1	3.80	0.58	0.4602
	BC	88.36	1	88.36	13.46	0.0028
	BD	21.16	1	21.16	3.22	0.0959
	CD	0.72	1	0.72	0.11	0.7454
	A^2	50.14	1	50.14	7.64	0.0161
	B^2	95.36	1	95.36	14.53	0.0022
	C^2	2.93	1	2.93	0.45	0.5155
	D^2	173.43	1	173.43	26.42	0.0002
	Residual	85.34	13	6.56		
	Lack of Fit	76.60	10	7.66	2.63	0.2306
	Pure Error	8.74	3	2.91		
	Cor Total	1750.95	29			
CR dye	Model	2524.16	14	180.30	26.95	< 0.0001
	A-pH	612.06	1	612.06	91.49	< 0.0001
	B-Dose	421.68	1	421.68	63.03	< 0.0001
	C-Ci	535.82	1	535.82	80.09	< 0.0001
	D-Time	433.50	1	433.50	64.80	< 0.0001
	AB	0.81	1	0.81	0.12	0.7334
	AC	7.02	1	7.02	1.05	0.3243
	AD	3.61	1	3.61	0.54	0.4756
	BC	6.25	1	6.25	0.93	0.3514
	BD	2.50×10^{-3}	1	2.50×10^{-4}	3.74×10^{-4}	0.9849
	CD	0.81	1	0.81	0.12	0.7334
	A^2	52.33	1	52.33	7.82	0.0151
	B^2	286.38	1	286.38	42.81	< 0.0001
	C^2	11.37	1	11.37	1.70	0.2150
	D^2	275.41	1	275.41	41.17	< 0.0001
	Residual	86.97	13	6.69		
	LOF	67.67	10	6.77	1.05	0.5474
	PE	19.31	3	6.44		
	Cor Total	2675.11	29			
MR dye	Model	2519.59	14	179.97	26.96	< 0.0001
	A-Initial pH	607.02	1	607.02	90.94	< 0.0001
	B-Dose	422.52	1	422.52	63.30	< 0.0001
	C-Ci	538.65	1	538.65	80.70	< 0.0001
	D-Time	434.35	1	434.35	65.07	< 0.0001
	AB	0.77	1	0.77	0.11	0.7403
	AC	6.63	1	6.63	0.99	0.3371
	AD	3.71	1	3.71	0.56	0.4695
	BC	5.88	1	5.88	0.88	0.3650
	BD	6.25×10^{-4}	1	6.25×10^{-4}	9.36×10^{-5}	0.9924
	CD	0.68	1	0.68	0.10	0.7546
	A^2	54.16	1	54.16	8.11	0.0137
	B^2	283.99	1	283.99	42.55	< 0.0001
	C^2	11.33	1	11.33	1.70	0.2152
	D^2	273.06	1	273.06	40.91	< 0.0001
	Residual	86.77	13	6.67		
	Lack of Fit	68.23	10	6.82	1.10	0.5279
	Pure Error	18.54	3	6.18		
	Cor Total	2673.59	29			

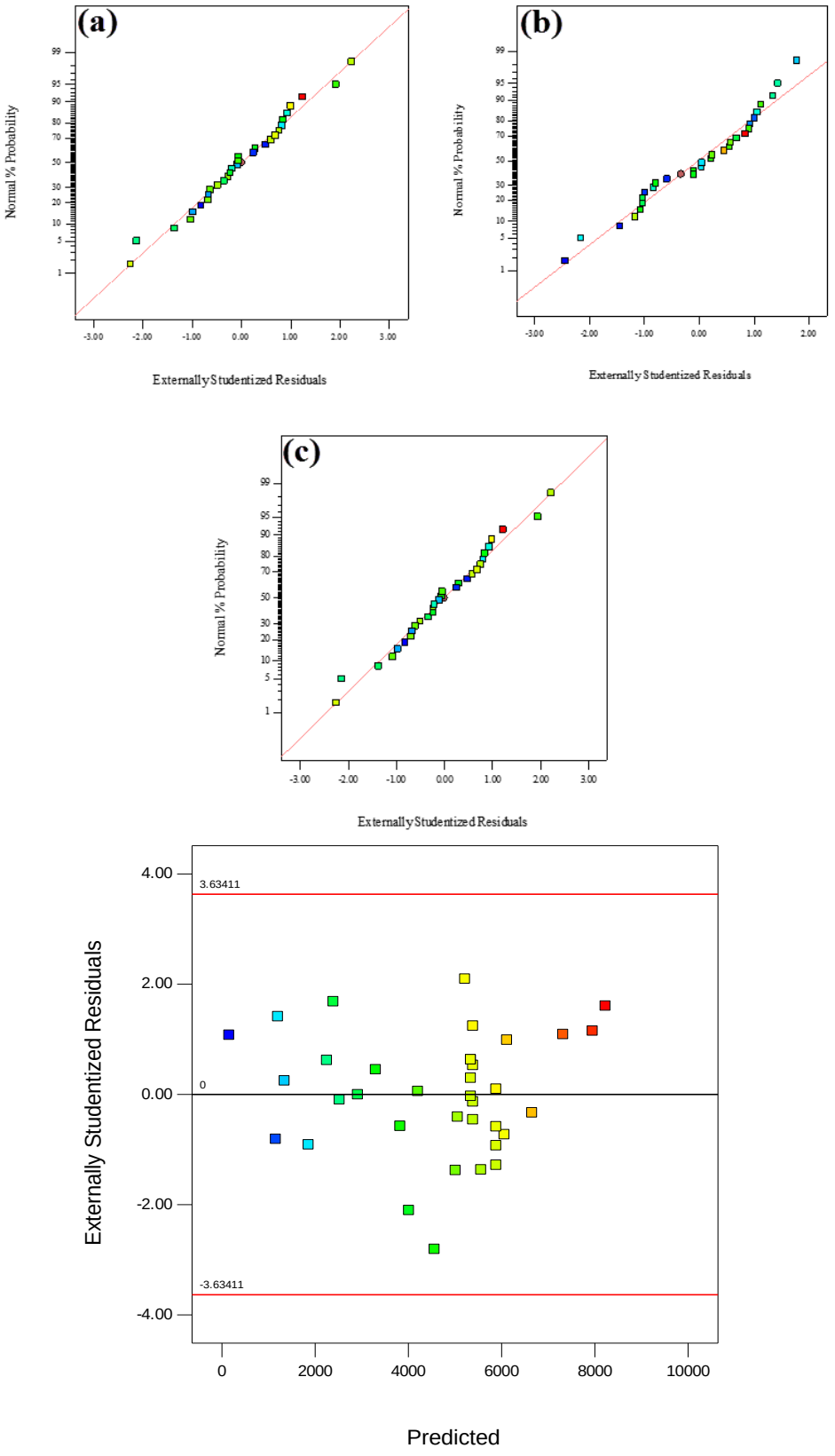

Fig. 6. Normal probability against externally studentized residuals for a) CR, b) MO and c) MR

3D plots of the model are very common tools for studying the interactions interpretation through visualization (Montgomery, 2012). Figs. 7, 8 and 9 show the plots of model response versus two experimental factors, while the value of other factors were fixed at their central levels. Figs. 7(a), 8(a), and 9(a) show the effects of medium pH and quantity of the Be@Fe-Cu, clearly indicating that the latter has a positive effects on the removal efficiency. In contrast, the efficiency increased with decreasing the pH to about 3.0 and then was constant. The lines in these Figs. are not parallel, indicating the presence of interactions between the quantity of the Be@Fe-Cu and medium pH.

The plot for the effects of medium pH and initial dye concentration on the degradation efficiency can be seen in Figs. 7(b), 8(b), and 9(b) which clearly shows that decreasing the initial concentration increased the efficiency. In this case no interactions were also observed between pH and the initial dye concentration.

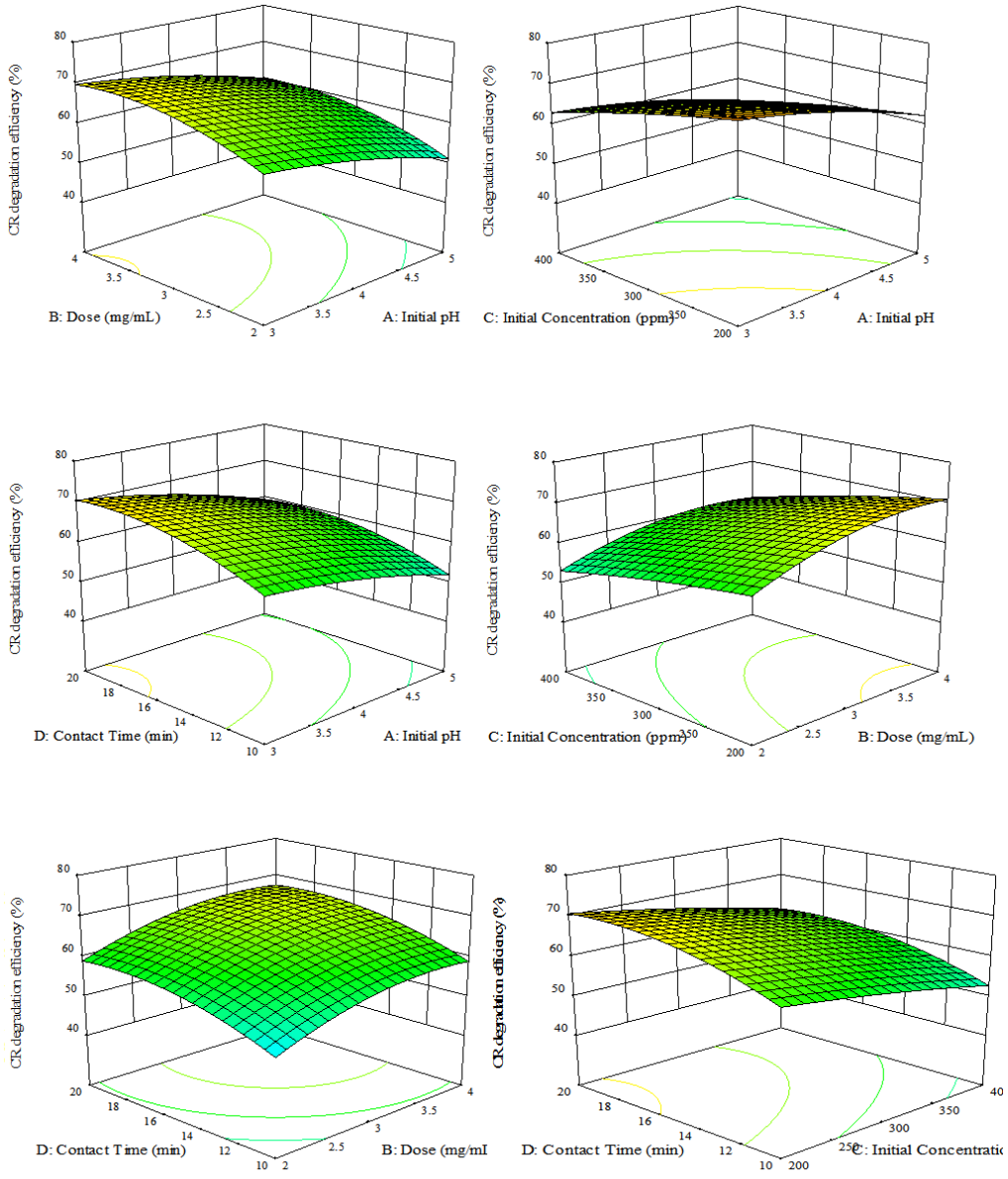

Fig. 7. 3D-plots for the proposed CR model.

In the case of sample pH and contact time (Figs. 7(c), 8(c), and 9(c)), the efficiency was found to increase with increasing the contact time, and these two factors were also found to be independent from each other. In a similar way no interactions were observed between the quantity of the Be@Fe-Cu and contact time (see Figs. 7(d), 8(d), and 9(d)).

The profiles in Figs. 7(e), 8(e), 9(e), 8(f), and 9(f) on the other hand, indicate no interaction between the contact time and initial dye concentration for CR, MO and MR, and also between the quantity of the Be@Fe-Cu and initial dye concentration in the case of CR and MO, which led to a non-linear relation between the response and these factors. However, these is an interaction between Be@Fe-Cu quantity and MO concentration. 3.2, and 44.7±5.7%, respectively).

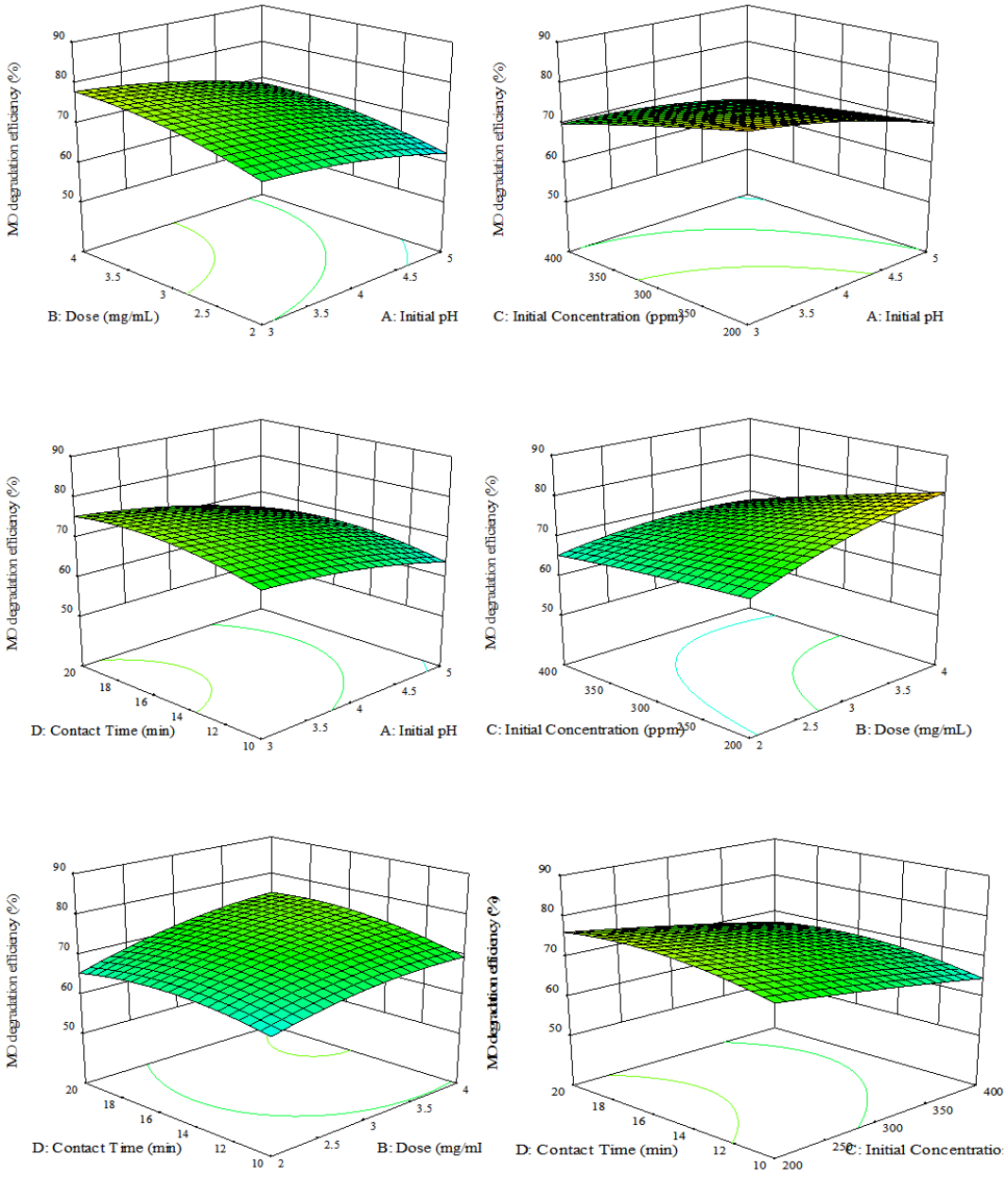

Fig. 8. 3D-plots for the proposed MO model.

Determining the optimal values of the effective factors to maximize the dye adsorption based on the model is the main goal of the optimization. This was done using the Design-Expert 10 (trial version) software and based on the non-linear optimization method, the optimal values of variables (i.e. medium pH, adsorbent quantity and contact time) were 3, 39 mg, 18 min at an initial dye concentration of 200 ppm. At a 95% confidence level, the best CR, MO, and MR degradation efficiency were predicted as 76.7±2.4, 85.1±2.5 and 47.3±1.7%, respectively, which was further verified by the experimental results obtained under optimized conditions (i.e. 71.1±3.2, 80.7±3.2, and 44.7±5.7%, respectively).

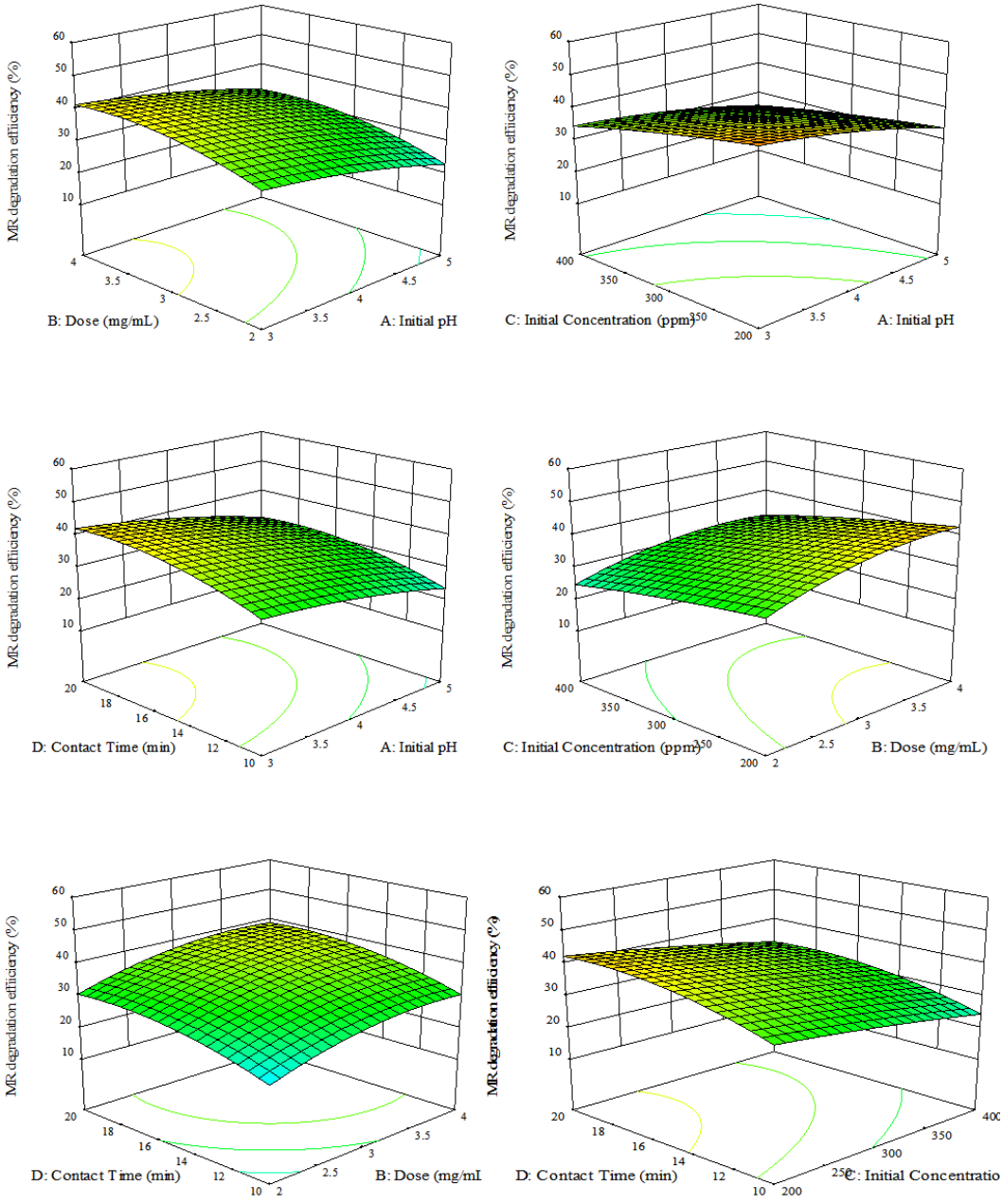

Fig. 9. 3D-plots for the proposed MO model.

CONCLUSION

In the present study, the use of bentonite as the support to develop Ben@Fe-Cu bi-metallic for CR, MO, and MR dyes reduction simultaneously from aqueous media are reported. Larger surface and higher dispersibility of Ben@Fe-Cu compared to unsupported are exhibited by incorporation of nZVI and Cu on the outer surface as well as within the inner pores. The characterization of prepared Ben@Fe-Cu was carried out by BET, XRD, TEM, FTIR, and SEM-EDX. The results demonstrate that the aggregation of nZVI nanoparticles could be effectively reduced by the bentonite and their reactivity towards the degradation of MO and CR could be enhanced. Optimizing the degradation process and maximizing efficiency were done using response surface methodology. With correlation coefficients of above 0.90 for CR, MO, and MR, the resulting models complied with the empirical data. It was found that reaching equilibrium takes place within 18 min for the process.

GRANT SUPPORT DETAILS

The present research did not receive any financial support.

CONFLICT OF INTEREST

The authors declare that there is not any conflict of interests regarding the publication of this manuscript. In addition, the ethical issues, including plagiarism, informed consent, misconduct, data fabrication and/ or falsification, double publication and/or submission, and redundancy has been completely observed by the authors.

LIFE SCIENCE REPORTING

No life science threat was practiced in this research.

REFERENCES

Allègre, C., Moulin, P., Maisseu, M. and Charbit, F. (2006). Treatment and reuse of reactive dyeing effluents. J. Memb. Sci., 269(1-2); 15-34.

Asfaram, A., Ghaedi, M., Azqhandi, M.H.A., Goudarzi, A. and Dastkhoon, M. (2016). Statistical experimental design, least squares-support vector machine (LS-SVM) and artificial neural network (ANN) methods for modeling the facilitated adsorption of methylene blue dye. RSC Adv., 6; 40502-40516.

Bao, B., Damtie, M.M., Hosseinzadeh, A., Wei, W., Jin, J., Vo, H.N.P., Ye, J.S., Liu, Y., Wang, X.F., Yu, Z.M., Chen, Z.J., Wu, K., Frost, R.L. and Ni, B.N. (2020). Bentonite-supported nano zero-valent iron composite as a green catalyst for bisphenol A degradation: Preparation, performance, and mechanism of action. J. Environ. Manage., 260; 110105-110113.

Behbahani, M., Barati, M., Bojdi, M.K., Pourali, A.R., Bagheri, A. and Tapeh, N.A.G. (2013). A nanosized cadmium(II)-imprinted polymer for use in selective trace determination of cadmium in complex matrices. Microchim. Acta., 180; 117-1125.

Behbahani, M., Esrafili, A., Bagheri, S., Radfar, S., Kalate Bojdi, M. and Bagheri, A. (2014). Modified nanoporous carbon as a novel sorbent before solvent-based de-emulsification dispersive liquid-liquid microextraction for ultra-trace detection of cadmium by flame atomic absorption spectrophotometry. Meas. J. Int. Meas. Confed., 51; 174-181.

Belessi, V., Romanos, G., Boukos, N., Lambropoulou, D. and Trapalis, C. (2009). Removal of Reactive Red 195 from aqueous solutions by adsorption on the surface of TiO2 nanoparticles. J. Hazard. Mater., 170(2-3); 836-844.

Bojdi, M.K., Mashhadizadeh, M.H., Behbahani, M., Farahani, A., Davarani, S.S.H. and Bagheri, A. (2014). Synthesis, characterization and application of novel lead imprinted polymer nanoparticles as a high selective electrochemical sensor for ultra-trace determination of lead ions in complex matrixes. Electrochim. Acta., 136; 59-65.

Chakraborty, A., Islam, D.A. and Acharya, H. (2019). One pot synthesis of ZnO-CuO nanocomposites for catalytic peroxidase like activity and dye degradation. Mater. Res. Bull., 120; 110592-110602.

Derringer, G. and Suich, R. (1980). Simultaneous Optimization of Several Response Variables. J. Qual. Technol., 12(4); 214-219.

Diao, Z.H., Xu, X.R., Jiang, D., Kong, L.J., Sun, Y.X., Hu, Y.X., Hao, Q.W. and Chen, H. (2016). Bentonite-supported nanoscale zero-valent iron/persulfate system for the simultaneous removal of Cr(VI) and phenol from aqueous solutions. Chem. Eng. J., 302; 213-222.

Hajjaji, W., Ganiyu, S.O., Tobaldi, D.M., Andrejkovičová, S., Pullar, R.C., Rocha, F. and Labrincha, J.A. (2013). Natural portuguese clayey

materials and derived TiO_2-containing composites used for decolouring methylene blue (MB) and orange II (OII) solutions. Appl. Clay Sci., 83-84; 91-98.

Hao, O.J., Kim, H. and Chiang, P.C. (2000). Decolorization of wastewater. Crit. Rev. Environ. Sci. Technol., 30(4); 449-505.

Jouali, A., Salhi, A., Aguedach, A., Aarfane, A., Ghazzaf, H., Lhadi, E.K., El krati, M. and Tahiri, S. (2019). Photo-catalytic degradation of methylene blue and reactive blue 21 dyes in dynamic mode using TiO2 particles immobilized on cellulosic fibers. J. Photochem. Photobiol. A Chem., 383; 112013-112021.

Karthiga, R., Kavitha, B., Rajarajan, M. and Suganthi, A. (2015). Photocatalytic and antimicrobial activity of NiWO4 nanoparticles stabilized by the plant extract. Mater. Sci. Semicond. Process., 40; 123-129.

Kurniawan, A., Sutiono, H., Indraswati, N. and Ismadji, S. (2012). Removal of basic dyes in binary system by adsorption using rarasaponin-bentonite: Revisited of extended Langmuir model. Chem. Eng. J., 189-190; 264-274.

Marković, M., Marinović, S., Mudrinić, T., Ajduković, M., Jović-Jovičić, N., Mojović, Z., Orlić, J., Milutinović-Nikolić, A. and Banković, P. (2019). Co(II) impregnated Al(III)-pillared montmorillonite–Synthesis, characterization and catalytic properties in Oxone® activation for dye degradation. Appl. Clay Sci., 182; 105276-105285.

Mittal, H. Ray, S.S. (2016). A study on the adsorption of methylene blue onto gum ghatti/TiO2 nanoparticles-based hydrogel nanocomposite. Int. J. Biol. Macromol., 88; 66-80.

Moghaddam, A.Z., Bojdi, M.K., Nakhaei, A., Ganjali, M.R., Alizadeh, T. and Faridbod, F. (2018). Ytterbium tungstate nanoparticles as a novel sorbent for basic dyes from aqueous solutions. Res. Chem. Intermed., 44; 6945-6962.

Moghaddam, A.Z., Jazi, M.E., Allahrasani, A., Ganjali, M.R. and Badiei, A. (2020). Removal of acid dyes from aqueous solutions using a new eco-friendly nanocomposite of $CoFe_2O_4$ modified with Tragacanth gum. J. Appl. Polym., Sci. 137(17); 48605-48617.

Montgomery, D.C. (2012). Design and Analysis of Experiments Eighth Edition, John Wiley & Sons Inc, Westford,.

O'Carroll, D., Sleep, B., Krol, M., Boparai, H. and Kocur, C. (2013). Nanoscale zero valent iron and bimetallic particles for contaminated site remediation. Adv. Water Resour., 51; 104-122.

Sabouri, M.R., Sohrabi, M.R. and Moghaddam, A.Z. (2020). A Novel and Efficient Dyes Degradation Using Bentonite Supported Zero-Valent Iron-Based Nanocomposites. ChemistrySelect, 5(1); 369-378.

Sahoo, A. and Patra, S. (2018). A Combined Process for the Degradation of Azo-Dyes and Efficient Removal of Aromatic Amines Using Porous Silicon Supported Porous Ruthenium Nanocatalyst. ACS Appl. Nano Mater., 1(9); 5169-5178.

Sahoo, A., Tripathy, S.K., Dehury, N. and Patra, S. (2015). A porous trimetallic Au@Pd@Ru nanoparticle system: Synthesis, characterisation and efficient dye degradation and removal. J. Mater. Chem. A, 3; 19376-19383.

Salama, A., Mohamed, A., Aboamera, N.M., Osman, T.A. and Khattab, A. (2018). Photocatalytic degradation of organic dyes using composite nanofibers under UV irradiation. Appl. Nanosci., 8; 155-161.

Shubair, T., Eljamal, O., Khalil, A.M.E., Tahara, A. and Matsunaga, N. (2018). Novel application of nanoscale zero valent iron and bimetallic nano-Fe/Cu particles for the treatment of cesium contaminated water. J. Environ. Chem. Eng., 6(4); 4253-4264.

Vijai Anand, K., Aravind Kumar, J., Keerthana, K., Deb, P., Tamilselvan, S., Theerthagiri, J., Rajeswari, V., Sekaran, S.M.S. and Govindaraju, K. (2019). Photocatalytic Degradation of Rhodamine B Dye Using Biogenic Hybrid ZnO-MgO Nanocomposites under Visible Light. ChemistrySelect, 4(17); 5178-5184.

Walsh, G.E., Bahner, L.H. and Horning, W.B. (1980). Toxicity of textile mill effluents to freshwater and estuarine algae, crustaceans and fishes. Environ. Pollution. Ser. A, Ecol. Biol., 21(3); 169-179.

Zeraatkar Moghaddam, A., Ghiamati, E., Pakar, R., Sabouri, M.R. and Ganjali, M.R. (2019). A novel and an efficient 3-D high nitrogen doped graphene oxide adsorbent for the removal of congo red from aqueous solutions. Pollution, 5; 501-514.

Zeraatkar Moghaddam, A., Ghiamati, E., Pourashuri, A. and Allahresani, A. (2018). Modified nickel ferrite nanocomposite/functionalized chitosan as a novel adsorbent for the removal of acidic dyes. Int. J. Biol. Macromol., 120; 1714-1725.